Kinetic interaction of cold and hot protons with an oblique EMIC wave near the dayside reconnecting magnetopause

S. Toledo-Redondo[1,2], J. H. Lee[3], S. K. Vines[4], D. L. Turner[4], R. C. Allen[4], M. André[5], S. A. Boardsen[6], J. L. Burch[7], R. E. Denton[8], H. S. Fu[9], S. A. Fuselier[7,10], D. J. Gershman[6], B. Giles[6], D. B. Graham[5], N. Kitamura[11], Yu. V. Khotyaintsev[5], B. Lavraud[2,12], O. LeContel[13], W. Y. Li[14], T. E. Moore[6], E. A. Navarro[15], J. Portí[16], A. Salinas[17], and A. Vinas[6]

[1]Department of Electromagnetism and Electronics, University of Murcia, Murcia, Spain.
[2]Institut de Recherche en Astrophysique et Planétologie, Université de Toulouse, CNRS, UPS, CNES, Toulouse, France.
[3]The Aerospace Corporation, El Segundo, CA, USA.
[4]The Johns Hopkins University Applied Physics Laboratory, Laurel, MD, USA.
[5]Swedish Institute of Space Physics, Uppsala, Sweden.
[6]NASA Goddard Space Flight Center, Greenbelt, Maryland, USA.
[7]Southwest Research Institute, San Antonio, Texas, USA.
[8]Department of Physics and Astronomy, Dartmouth College, Hanover, New Hampshire, USA.
[9]School of Space and Environment, Beihang University, Beijing, China.
[10]University of Texas at San Antonio, San Antonio, Texas, USA.
[11]Department of Earth and Planetary Science, Graduate School of Science, University of Tokyo, Tokyo, Japan.
[12]Laboratoire d'Astrophysique de Bordeaux, Univ. Bordeaux, CNRS, B18N, allée Geoffroy Saint-Hilaire, 33615 Pessac, France
[13]Laboratoire de Physique des Plasmas (LPP), UMR7648 CNRS/Ecole Polytechnique Institut Polytechnique de Paris/Sorbonne Université/Université Paris Saclay/Observatoire de Paris, Paris, France
[14]State Key Laboratory of Space Weather, National Space Science Center, Chinese Academy of Sciences, Beijing, 100190, China.
[15]Department of Applied Physics, Universitat de Valencia, Valencia, Spain.
[16]Department of Applied Physics, University of Granada, Granada, Spain.
[17]Department of Electromagnetism and Matter Physics, University of Granada, Granada, Spain.

Key Points:

- In-situ observations of different dynamics of cold (eV) and hot (keV) protons inside an EMIC wave
- Wave number estimation shows that cold protons behave as fluid while hot protons interact at kinetic scales
- Magnetized cold protons modify the Ohm's law balance and favor propagation at large wave normal angle

Corresponding author: S. Toledo-Redondo, `sergio.toledo@um.es`

Abstract

We report observations of the ion dynamics inside an Alfvén branch wave that propagates near the reconnecting dayside magnetopause. The measured frequency, wave normal angle and polarization are within 1% with the predictions of a dispersion solver, and indicate that the wave is an electromagnetic ion cyclotron wave with very oblique wave vector. The magnetospheric plasma contains hot protons (keV), cold protons (eV), plus some heavy ions. The cold protons follow the magnetic field fluctuations and remain frozen-in, while the hot protons are at the limit of magnetization. The cold proton velocity fluctuations contribute to balance the Hall term in Ohm's law, allowing the wave polarization to be highly-elliptical and right-handed, a necessary condition for propagation at oblique wave normal angles. The dispersion solver indicates that increasing the cold proton density facilitates generation and propagation of these waves at oblique angles, as it occurs for the observed wave.

Plain Language Summary

The Earth's magnetosphere is a very dilute cloud of charged particles which are trapped in the Earth's magnetic field. This cloud is surrounded by the solar wind, another very dilute gas that flows supersonically throughout the solar system. These two plasmas can couple to each other via magnetic reconnection, a fundamental plasma process that occurs at the dayside region of the interface between the two plasmas. When reconnection occurs, large amounts of energy and particles enter the magnetosphere, driving the near Earth space dynamics and generating, for instance, aurorae. The magnetospheric plasma sources are the solar wind and the Earth's ionosphere. Multiple plasma populations can be found inside the Earth's magnetosphere, depending on the plasma origin and its time history, as well as the magnetospheric forcing of the solar wind. In this study, we show how the presence of multiple particle populations at the interface between the solar wind and the magnetosphere modify the properties of the waves that propagate there. Waves are known to play a fundamental role in converting energy and heating these very dilute charged gas clouds.

1 Introduction

Electromagnetic Ion Cyclotron (EMIC) waves are generated in various regions of the Earth's magnetosphere when hot (keV to tens of keV) ions have $T_\perp > T_{||}$ (e.g., Kennel & Petschek, 1966; Gary & Winske, 1990; Gary, 1992). The wave growth rate maximizes in regions of **B** minima (e.g., Allen et al., 2015). EMIC waves are thought to grow at parallel wave normal angles (θ_{Bk}) and exhibit left-handed polarization, but it is common to observe them propagating with large θ_{Bk}, and this is associated with a departure from left-handed polarization (e.g., Min et al., 2012; Allen et al., 2015).

One possible way of departing from left-handed polarization is propagation near the crossover frequency when heavy ions are present (Denton et al., 1996). Oblique propagation ($\theta_{Bk} > 30°$) is generally associated with linear and right-handed polarizations (B. J. Anderson et al., 1996). Hu and Denton (2009); Omidi et al. (2011) showed that propagation along the **B** field gradients of the Earth's dipole leads to oblique propagation of EMIC waves due to the changing refraction index, and that the waves are reflected when they reach the local bi-ion frequency. However, for oblique propagation, it is expected that the wave is strongly damped (Thorne & Horne, 1993). B. J. Anderson et al. (1992) observed that most EMIC waves in the dawn-sector exhibited linear polarization that could not be explained only by propagation near the crossover frequency along a magnetic field gradient. Hu et al. (2010) showed, using 2.5D hybrid simulations, that the waves could be generated at oblique angles, in particular when there is a small amount

of heavy ions and a large amount of cold protons, in addition to hot anisotropic protons which provide the energy source.

The Magnetospheric Multiscale (MMS) mission (Burch et al., 2015) provides unprecedented high-resolution measurements in the near-Earth plasma environment which have enabled studying the kinetic interaction of cold and hot protons in detail, and have recently showed the cold proton ability to remain magnetized inside spatial structures larger than their gyroradius (André et al., 2016; Toledo-Redondo et al., 2016; Toledo-Redondo et al., 2018; Alm et al., 2019; Shi et al., 2020). In this work, we observe an EMIC wave propagating with a very oblique wave vector, and show that hot and cold protons interact with the wave electromagnetic fields in a kinetic and fluid sense, respectively. The temperature anisotropy of the hot protons drives the instability which generates the EMIC wave, and their gyroradius is comparable to the wavelength. On the other hand, the cold protons have a gyroradius well below the wavelength, allowing them to remain frozen-in and follow the fluctuations imposed by the slowly varying fields of the waves, self-consistently favoring wave propagation at oblique angles.

2 EMIC wave environment

On the 24th of October 2015, at 15:26 UT, the MMS fleet (Burch et al., 2015) was in the dayside magnetosphere at (7.3, 8.0, -0.8) Earth radii (R_E) in Geocentric Solar Ecliptic (GSE) coordinates (MLAT = -23°, L-shell = 12.8) and crossed the magnetopause multiple times. When the fleet re-entered the magnetosphere, it observed a wave for ∼20 s. Figure 1a shows the magnetic field in GSE coordinates (Russell et al., 2014). From 15:27:25 UT onwards, marked by yellow shading, **B** fluctuations caused by the wave are observed. Figure 1b shows the electric field measurements in GSE coordinates (Lindqvist et al., 2014; Ergun et al., 2014). Electric fields of ∼10 mV/m consistent with separatrix crossings are observed on the magnetospheric edges of the magnetopause. Electric field fluctuations associated with the wave are observed from 15:27:25 UT onwards. Figure 1c shows the total ion (black), electron (blue), He^+ (red), He^{2+} (green) and O^+ (gray) number densities recorded by the Fast Plasma Investigation (FPI) (Pollock et al., 2016) and the Hot Plasma Composition Analyzer (HPCA) (Young et al., 2014). The total density in the magnetosphere is roughly 1 cm^{-3}, mainly contributed by cold and hot protons. The measured electron density goes below 1 cm^{-3} and deviates from the ion density towards the end of the interval. The reason is likely the presence of cold electrons below the 10 eV threshold of FPI. During the entire interval of Figure 1, the spacecraft was charged positively below 10 V. Figure 1d shows the ion velocity (GSE) recorded by FPI. We observe an ion flow in the -$\mathbf{z}_{GSE}$ direction that peaks at -250 km/s, corresponding to 1.1 v_A, where v_A is the observed hybrid Alfvén velocity at the magnetopause (Cassak & Shay, 2007). The ion flow and the electric field separatrix signatures indicate that reconnection may be occurring at the magnetopause, with the X line located northward of the spacecraft, consistent with the maximum shear model predictions at that time (Trattner et al., 2007). At the end of the time interval, the magnetopause is moving sunward at a peak velocity of ∼150 km/s. Figure 1e shows an ion energy spectrogram, where three populations can be distinguished. In the magnetosphere, there is a hot population with energies above 2 keV, the plasma sheet ions, plus a cold population with total energies of 50 - 300 eV of ionospheric origin. The black line is the equivalent $\mathbf{E}\times\mathbf{B}$ energy for protons. The total cold ion energy is greater than a few eV due to the relative motion of the ambient plasma with respect to the spacecraft. The third one is the ion population with energies from a few tens of eV up to a few keV from the magnetosheath. The total parallel ($T_{i||}$) and perpendicular ($T_{i\perp}$) temperatures are shown using green and blue lines, respectively. The cold ion heating observed between 15:27:10 - 15:27:20 UT has been previously studied by Toledo-Redondo et al. (2017). From 15:27:20 UT onwards, the cold ion energy fluctuates up and down as a consequence of the interaction with the wave. Figure 1f shows the electron energy spectrogram recorded by FPI Dual Electron

Spectrometers (DES). As for the ions, three populations can be distinguished based on their energies: plasma sheet electrons, cold electrons of ionospheric origin, and magnetosheath electrons. Figure 1g shows the magnetic field dynamic spectrum in the low frequency (0.1 - 6 Hz) band. The magnetic field fluctuations observed after 15:27:20 UT have a peak in power at ∼0.35 Hz in the spacecraft frame, below the H^+ and above the He^+ cyclotron frequency bands.

3 Observed wave properties

We now focus on the low-frequency wave observation ($f_{sc} \sim 0.35$ Hz) in the yellow-shaded interval of Figure 1, 15:27:25 - 15:27:44 UT. Figure 2a shows the ion energy spectrogram recorded by FPI in the low-energy range, averaged among the four MMS spacecraft. The equivalent $\mathbf{E}\times\mathbf{B}$ energy for protons is plotted in black. The energy of the cold ion population fluctuates periodically between tens of eV and few hundred eV. For most of the interval, the average energy of the cold ions is above 50 eV, except for the last 3 - 4 s. Therefore, the FPI-ion and $\mathbf{E}$ field measurements are in general only weakly affected by the sheath electrostatic potential of the spacecraft and the formation of cold ion wakes, except for the last 3 - 4 s, where the effect may be substantial (Toledo-Redondo et al., 2019). We computed partial moments (e.g., Toledo-Redondo et al., 2016; Li et al., 2017; Lee et al., 2019) for the cold (10 - 400 eV) and hot (2 - 40 keV) ion populations on each of the four MMS spacecraft. The MMS fleet is in tetrahedron formation with a spacecraft separation of ∼ 15 km, much smaller than the characteristic wavelength (λ) of the wave under study (see below). Figure 2b shows the electron density fluctuations (Δn_e) from FPI, and the partial cold and hot ion density fluctuations (Δn_{ic}, Δn_{ih}), averaged among the 4 spacecraft. Density fluctuations (Δn) are computed using a 5th order elliptical band-pass filter, with cutoff frequencies at $0.1 f_{H^+}$ and $5 f_{H^+}$, where f_{H^+}= 0.57 Hz, corresponding to the proton cyclotron frequency in the interval 15:27:25 - 15:27:44 UT. Fluctuations (Δ) of any quantity throughout the study are computed using the same filtering. The total ion and electron density is ∼1 cm^{-3} (Figure 1c). The number density of the heavy ion species contributes less than 10%, and most of the ions correspond to protons, of which approximately one half correspond to hot protons and one half to cold protons (not shown). There is a fluctuation of the electron and cold proton density of ∼0.1 cm^{-3} (i.e., 20% of the cold proton density) that is not observed for the hot protons. We apply Maximum Variance Analysis (MVA) to $\Delta\mathbf{B}$ and obtain $\hat{\mathbf{e}}_{\perp 1}$= (0.98, -0.12, -0.16) in GSE. Another perpendicular direction to $\mathbf{B}$ is obtained applying MVA to $\Delta\mathbf{E}$ field fluctuations. The parallel direction is defined as the cross product of the two perpendicular directions: $\hat{\mathbf{e}}_{||}$= (0.18, 0.14, 0.97) in GSE. Finally, $\hat{\mathbf{e}}_{\perp 2}=\hat{\mathbf{e}}_{||}\times\hat{\mathbf{e}}_{\perp 1}$ = (0.09, 0.998, -0.15) in GSE. The parallel direction defined in this way has an angle $< 5^\circ$ with the average $\mathbf{B}$ direction in the wave interval. The system ($\hat{\mathbf{e}}_{||}$, $\hat{\mathbf{e}}_{\perp 1}$, $\hat{\mathbf{e}}_{\perp 2}$) defines the Field-Aligned Coordinates (FAC) used in this study. $\Delta\mathbf{B}$ and $\Delta\mathbf{E}$ are plotted in Figures 2c and 2d respectively. The black vertical lines in Figure 2 indicate $\Delta B_{\perp 1}$ maxima. $\Delta\mathbf{B}$ exhibits highly elliptical, right-handed polarization, with L2/L1 ∼ 0.26, where L2 and L1 are the eigenvalues of the intermediate and maximum directions obtained by MVA, respectively. We compute the fluctuations of the Ohm's law terms, for a three fluid plasma including electrons, cold protons and hot protons (Toledo-Redondo et al., 2015):

$$\Delta\mathbf{E} = -\Delta\left(\frac{n_{ic}}{n}\mathbf{v_{ic}}\times\mathbf{B}\right) - \Delta\left(\frac{n_{ih}}{n}\mathbf{v_{ih}}\times\mathbf{B}\right) + \Delta\left(\frac{1}{en}\mathbf{J}\times\mathbf{B}\right) - \Delta\left(\frac{1}{en}\nabla\cdot\mathbf{P_e}\right), \quad (1)$$

where $\mathbf{J}$ was obtained using the curlometer technique (Dunlop et al., 1988). The heavy ion convection terms can be neglected due to their small number densities. Inside the magnetosphere, the electron density is small (∼1 cm^{-3}) and the electron temperature is large (hundreds of eV), and we cannot reliably obtain the $\nabla\cdot\mathbf{P_e}/en$ term, although we expect it to be small. Although MMS observed two electron populations in the magnetosphere, we treat them as a single population for simplification, since we do not expect a differential behavior of the two populations at the time and spatial scales of the

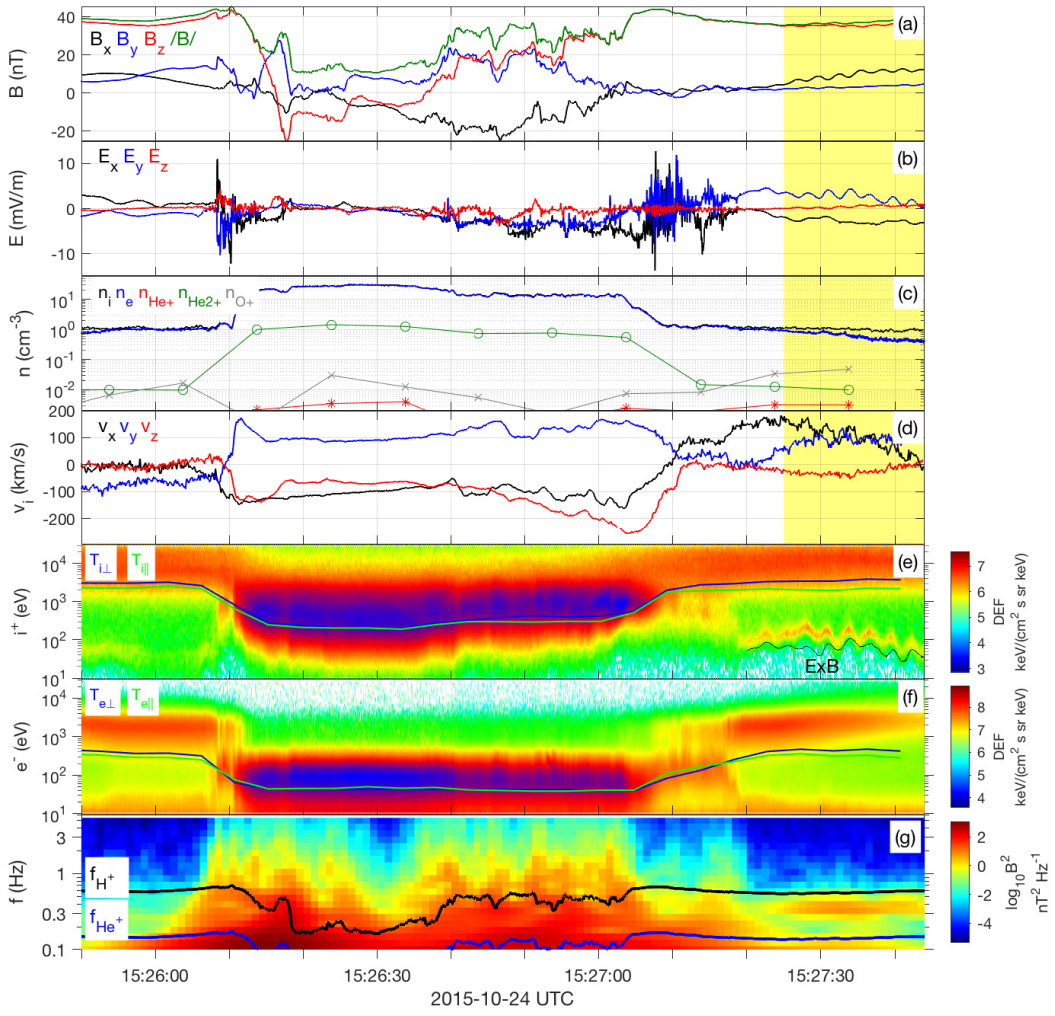

Figure 1. Overview of the MMS1 magnetopause crossing. (a) Magnetic field in GSE coordinates. (b) Electric field in GSE coordinates. (c) (black) Number densities of all ions from FPI, (blue) electrons from FPI, (red, green and gray) and heavy ions (He^+, He^{2+} and O^+) from HPCA. (d) FPI ion velocity in GSE coordinates. (e) (color) FPI Ion Differential Energy Flux (DEF), (black) equivalent $\mathbf{E}\times\mathbf{B}$ energy for protons, (blue) perpendicular ion temperature ($T_{i\perp}$), (green) parallel ion temperature ($T_{i||}$). (f) FPI electron DEF, (blue) perpendicular electron temperature ($T_{e\perp}$), (green) parallel electron temperature ($T_{e||}$). (g) (color) Magnetic field spectrogram, (black) H^+ cyclotron frequency, (blue) He^+ cyclotron frequency.

wave. This is confirmed using a wave dispersion solver, which yielded the same results for the Alfvén branch when accounting for a single or double electron population (cf. section 3). The $\hat{\mathbf{e}}_{\perp 2}$ components of the fluctuations of the Ohm's law right-hand side terms are plotted in Figure 2e. The main contributions are provided by the cold ion convection term and the Hall term, and to a lesser degree by the hot ion convection term. The sum of the right-hand side terms of equation 1 is also plotted in Figure 2d (green dashed line). The agreement between the measured electric field fluctuations and the sum of the right-hand side terms of equation (1) is very good, except for the last 3 s of the time interval of Figure 2, when the cold ion energy is lower and both **E** and FPI-ion measurements become less reliable owing to the electrostatic potential structure of the spacecraft and ion wake effects (Toledo-Redondo et al., 2019). We performed a linear regression analysis between $\Delta\mathbf{E}$ and -$\Delta\mathbf{v_{ic}}\times\mathbf{B}$ in the $\hat{\mathbf{e}}_{\perp 2}$ direction, and found a correlation coefficient $r = 0.85$ (Figure 2k), for the time interval of Figure 2 excluding the last 3 s, while the correlation between $\Delta E_{\perp 2}$ and -$\Delta(\mathbf{v_{ih}} \times \mathbf{B})_{\perp 2}$ was $r = 0.44$ (Figure 2j). This suggests that cold ions are magnetized and follow $\mathbf{E}\times\mathbf{B}$ motion, while hot ions are less magnetized. Figure 2f shows the Ohm's law terms in the $\hat{\mathbf{e}}_{\perp 1}$ direction. The net $\Delta E_{\perp 1}$ field is negligible ($\Delta E_{\perp 1} \sim 0.1\Delta E_{\perp 2}$) (blue and red curves in Figure 2d), consistent with the highly elliptical polarization of the wave. This results from the non-negligible contributions of the cold ion convection term and the Hall term in the $\perp$ 1 direction (black and red curves in Figure 2f), which roughly cancel each other. The correlation coefficient between the fluctuations of the cold ion convection term, $\Delta(n_{ic}/n(\mathbf{v_{ic}} \times \mathbf{B}))_{\perp 1}$ (black curve in Figure 2f), and the Hall term, $\Delta(\mathbf{J}\times\mathbf{B}/en)$ (red curve in Figure 2f), in the $\hat{\mathbf{e}}_{\perp 1}$ direction is $r = 0.79$ (Figure 2m), while the correlation between $\Delta(n_{ih}/n(\mathbf{v_{ih}}\times\mathbf{B}))_{\perp 1}$ and $\Delta(\mathbf{J} \times \mathbf{B}/en)_{\perp 1}$ is 0.23 (Figure 2l). The implications of the cold ion term in balancing the electric field fluctuations are discussed in section 4. We compute the associated speed of the field fluctuations RMS($\Delta E/\Delta B$ = 750 km/s), where RMS stands for Root Mean Squared. The associated Alfvén velocity of the interval is v_A= 770 km/s (B = 36 nT, n = 1 cm^{-3}), indicating that the wave likely corresponds to the Alfvénic branch. The currents are calculated using two methods: the curlometer and from plasma moments at each spacecraft, and averaged among the four spacecraft. Figure 2g shows $\Delta J_{||}$ from the two methods, which are roughly consistent. The parallel current is roughly at 90° phase shift with respect to $\Delta B_{\perp 1}$. Figure 2h shows a magnetic field spectrogram. The wave power is located between the He^+ (blue line) and the H^+ (black line) cyclotron bands, at ∼0.35 Hz in the spacecraft frame, see also Figure 1g. Magnetic field polarization analysis shows that the angle between the wave vector **k** and the background magnetic field, θ_{Bk} is ∼70° (Figure 2i). Bellan (2016) presented a method to compute the **k** vector of low-frequency waves if the current density vector **J** is known. It is based on the Ampere's law in the frequency domain, assuming a monochromatic wave: $\mu_0\mathbf{J}(\omega) = i\mathbf{k}(\omega)\times\mathbf{B}(\omega)$. Following that procedure and calculating the fluctuations of the current density vector $\Delta\mathbf{J}$ using the curlometer technique, we obtain $\mathbf{k}_{Bellan}$ = (1.9, 0.6, 5.6)·10^{-3} rad/km in FAC ($\hat{\mathbf{e}}_{||}$, $\hat{\mathbf{e}}_{\perp 1}$, $\hat{\mathbf{e}}_{\perp 2}$). We also compute the **k** vector from four-spacecraft cross-correlations and time differencing analysis of the magnetic field (Balikhin et al., 2003; Pinçon & Glassmeier, 2008). We obtain a very similar result, $\mathbf{k}_{4sc}$ = (2.2, 0.3, 5.1)·10^{-3} rad/km in FAC, corresponding to a difference of less than 6° from $\mathbf{k}_{Bellan}$. We assumed the wave to be monochromatic with a frequency of 0.35 Hz in the spacecraft frame, corresponding to the frequency where the magnetic field spectrum peaks. More details of these calculations can be found in Figure S1 of the supplemental material. We conclude that the angle between **B** and **k** is $\theta_{Bk} \sim 72°$, as indicated by three independent methods. The median bulk ion velocity during the interval of the wave observation, 15:27:25 - 15:27:44 UT, is $\mathbf{v}_0$ = (98, 95, -27) km/s in GSE. After correction for the doppler shift effect ($f_{wave} = f_{sc} - \mathbf{k}\cdot\mathbf{v}_0/2\pi$), the frequency of the wave in the plasma frame is found to be f_{wave} = 0.26 Hz, i.e. roughly 0.5f$_{H^+}$.

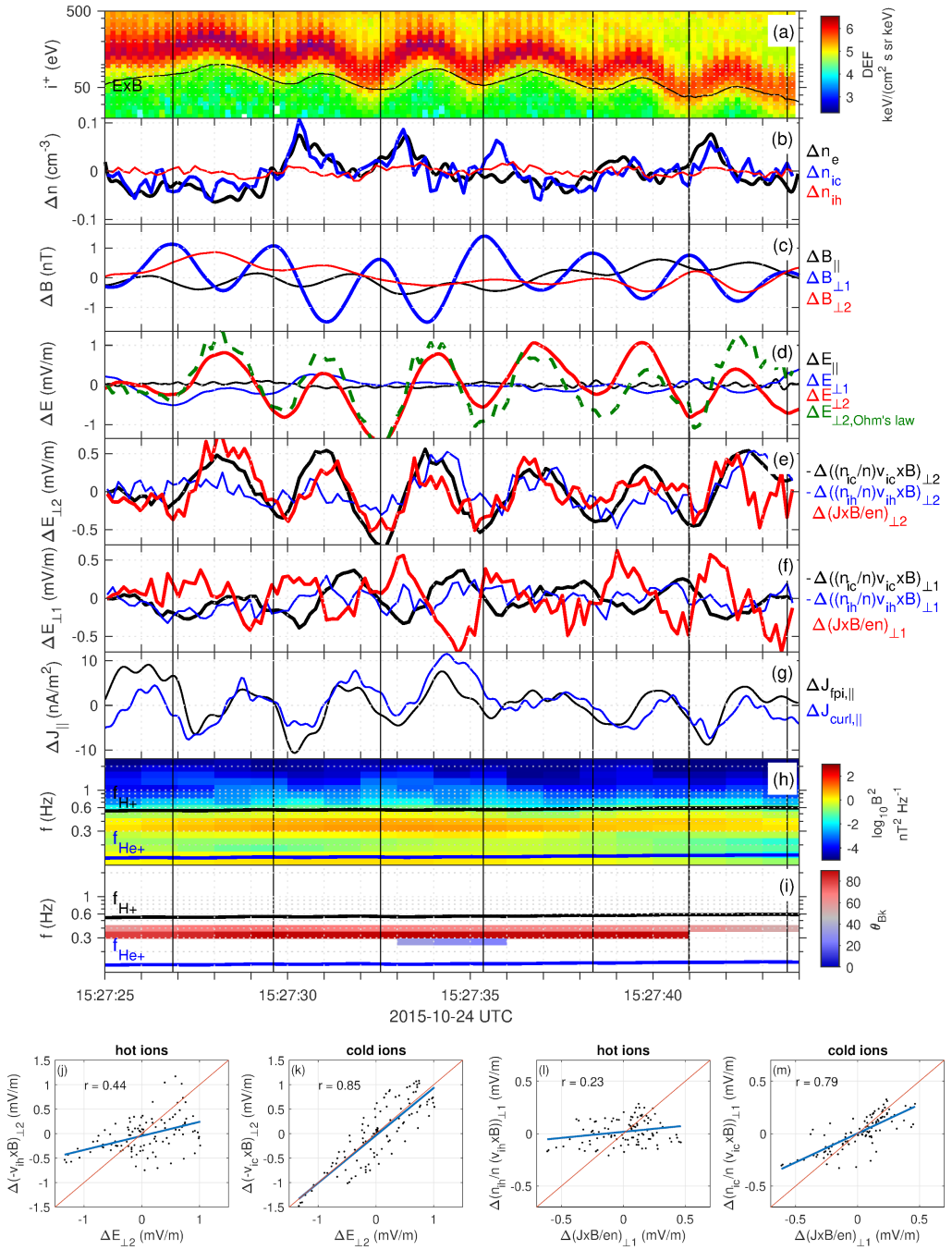

Figure 2. EMIC wave observation in the interval 15:27:25 UT - 15:27:44 UT. All panels correspond to four spacecraft averages. Vertical black lines indicate the peaks in $\Delta B_{\perp 1}$. (a) (color) FPI Ion energy spectrogram in DEF, (black) equivalent $\mathbf{E}\times\mathbf{B}$ energy for protons, (b) Density fluctuations for electrons (Δn_e, black), cold magnetospheric ions (Δn_{ic}, blue), and hot magnetospheric ions (Δn_{ih}, red). (c) Magnetic field fluctuations ($\Delta\mathbf{B}$) in FAC. (d) Electric field fluctuations ($\Delta\mathbf{E}$) in FAC and sum of the right-hand side terms of equation (1) for the $\hat{\mathbf{e}}_{\perp 2}$ direction. (e) Ohm's law terms for the $\hat{\mathbf{e}}_{\perp 2}$ direction. (f) Ohm's law terms for the $\hat{\mathbf{e}}_{\perp 1}$ direction. (g) Parallel component of the current density fluctuations ($\Delta\mathbf{J}$), measured from FPI moments (black) and from curlometer (blue). (h) Magnetic field power spectral density measured by MMS1 near the H^+ and He^+ cyclotron frequencies (black and blue lines, respectively). (i) Angle between magnetic field and wave vector, θ_{Bk}, for power spectral densities >1 nT^2Hz^{-1}. (j) Linear regression analysis of $\Delta\mathbf{E}$ and -$\Delta(\mathbf{v}_{ih}\times\mathbf{B})$ in the $\hat{\mathbf{e}}_{\perp 2}$ direction. (k) Linear regression analysis of $\Delta\mathbf{E}$ and -$\Delta(\mathbf{v}_{ic}\times\mathbf{B})$ in the $\hat{\mathbf{e}}_{\perp 2}$ direction. (l) Linear regression analysis of $\Delta(\mathbf{J}\times\mathbf{B}/en)$ and $\Delta n_{ih}/n(\mathbf{v}_{ih}\times\mathbf{B})$ in the $\hat{\mathbf{e}}_{\perp 1}$ direction. (m) Linear regression analysis of $\Delta(\mathbf{J}\times\mathbf{B}/en)$ and $\Delta n_{ic}/n(\mathbf{v}_{ic}\times\mathbf{B})$ in the $\hat{\mathbf{e}}_{\perp 1}$ direction.

4 Modelled wave properties

Next, we model the wave using Waves in Homogeneous Anisotropic Magnetized Plasma (WHAMP) (Roennmark, 1982), accounting for the populations measured by MMS: O^+, He^{2+}, He^+, cold H^+, hot H^+, and electrons. Their density, temperature and anisotropy are taken from the average value in the time interval of Figure 2. There is no strong background current during the event, so the relative drift velocities between populations are set to zero for all species and there are no ion-ion instability effects. The average plasma parameters of each population can be found in Table S1 of the supplemental material. Accounting for a cold electron population has no significant effects over the branch of interest, i.e. the Alfvén branch. If heavy ions are not included in the model, the dispersion surface is slightly modified, but the growth rate and polarization are not significantly changed, for the **k** vector and frequency measured by MMS. The results of the dispersion solver for the Alfvén branch near f_{H^+}, including 5 ion populations plus electrons, are shown in Figures 3a-d. Panel 3a shows the normalized frequency (Ω/Ω_i), where $\Omega_i = 2\pi f_{H^+}$, as a function of normalized $k_{||}$ ($k_{||}\rho_{ih}$), where ρ_{ih} is the hot ion gyroradius, for $k_\perp\rho_{ih} = 0$ and 1.96 (red and black lines), corresponding to $\theta_{Bk} = 0°$ and 72° at the measured $k_{||}$, respectively. The green asterisk corresponds to the normalized frequency measured by MMS and corrected for doppler shift, and is within 1% of the prediction (the accuracy drops to 5% if heavy ions are not accounted for in the model). Figure 3b is similar to 3a, but the vertical axis represents the normalized growth rate (γ/Ω_i) . The growth rate is positive for $\theta_{Bk} = 0°$, and becomes slightly negative at the measured wave normal angle $\theta_{Bk} = 72°$. Figure 3c shows the growth rate along the dispersion surface of the Alfvén branch. For the observed frequency (green asterisk) and θ_{Bk}, the wave is slightly damped, but we note that for $\theta_{Bk} \leq 50°$ the growth rate becomes positive. Figure 3d is similar to 3c but the colormap indicates the ellipticity $\epsilon = \mathrm{Re}(iB_{\perp 2}/B_{\perp 1})$. Values close to 1 indicate circular, Right-Handed Polarization (RHP). The dispersion solver predicts an ellipticity $\epsilon = 0.24$, i.e., within 1% of the measured ellipticity.

We present three runs with varying amounts of cold protons ($n_{ic} = 0.01$, 0.1 and 1 cm^{-3}) in Figures 3e-g, where the hot proton population has been left unchanged, and the electron population provides quasi-neutrality. For simplicity, we did not include heavy ion populations in these runs. The hot proton parameters for the three runs are $n_{ih} = 0.5$ cm^{-3}, $T_{||} = 4.4$ keV and $T_\perp/T_{||} = 1.8$. Other plasma parameters are provided in Table S2 of the supplemental material. The growth rate, ellipticity (ϵ) and wave normal angle (θ_{Bk}), as a function of $k_\perp\rho_{ih}$ are plotted in Figures 3e-g, in the regions where growth rate is positive. $k_{||}$ is chosen to maximize growth rate when $k_\perp$ is zero. For any given **k**, frequency variations are of the order of 10% between runs. Positive growth rate is larger and occurs over a larger frequency range when more cold protons are present, despite that the source of energy, i.e., hot proton temperature anisotropy, remains constant (Gary et al., 1994). The largest growth rate is observed for small $k_\perp\rho_{ih}$, but large and positive growth rate for large $k_\perp\rho_{ih}$ is present when cold H^+ density is large (red curves in Figure 3e). The run with $n_{ic} = 1$ cm^{-3} has positive growth rate for $\theta_{Bk} > 60°$ (Figure 3g), and shows highly elliptical right-handed polarization (Figure 3f), similar to the properties of the wave observed by MMS.

5 Discussion and Conclusions

The measured frequency and ellipticity are in excellent agreement with a numerical dispersion solver (within 1%), and the solver indicates that the wave was slightly damped for the observed frequency and wave vector. A comparison of three runs varying the cold proton number density indicates that they enable positive growth rates at large wave normal angles, consistent with the hybrid simulations in Hu et al. (2010). A careful examination of the **E** field fluctuations and the contributions by the Ohm's law terms reveal that cold protons are fully magnetized while hot protons are, to a certain extent, demagnetized, i.e., do not follow $\mathbf{E}\times\mathbf{B}$ drift. The fluctuations of the cold ion term and the Hall

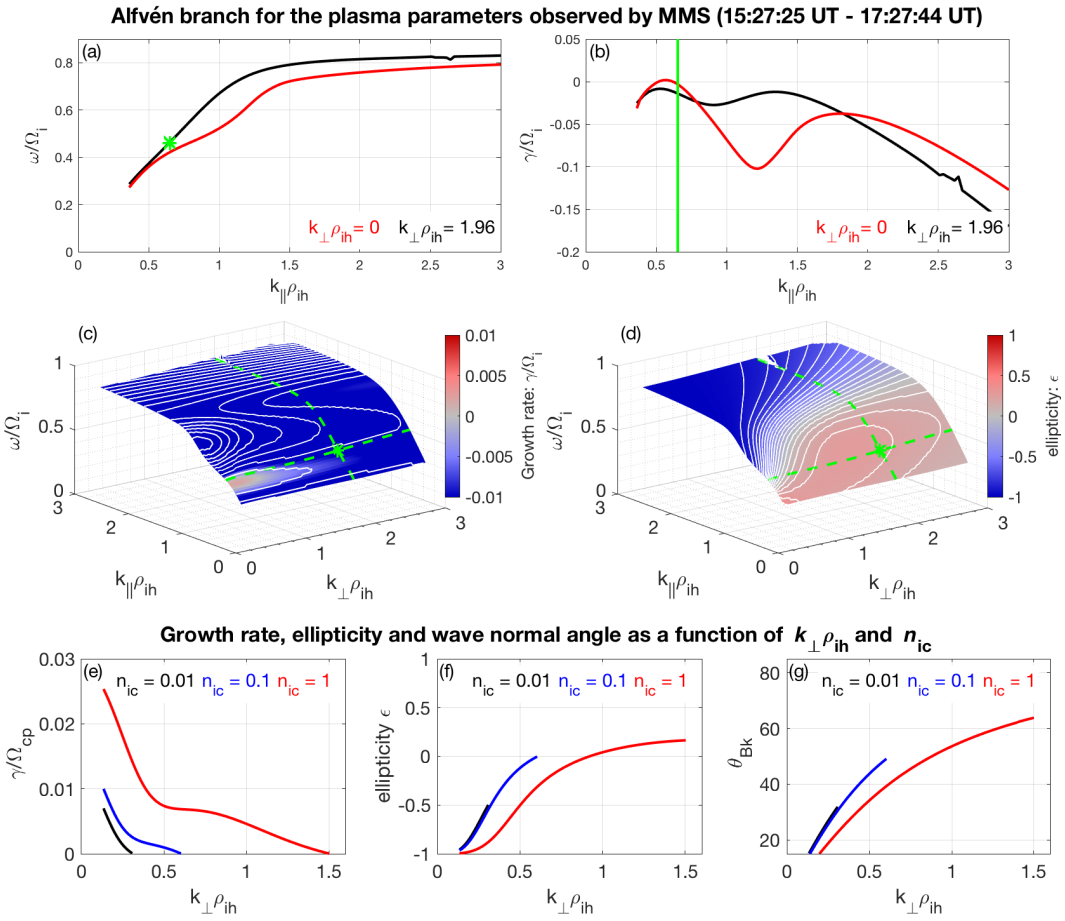

Figure 3. (a-d) Dispersion relation of the Alfvén branch corresponding to the plasma parameters measured by MMS in the interval 15:27:25 - 15:27:44 UT. The plasma parameters are specified in Table S1 of the supplemental material. (a) Normalized frequency (Ω/Ω_i) as a function of the normalized parallel component of the wavevector ($k_{||}\rho_{ih}$), for $k_\perp\rho_{ih} = 0$ (red), and the observed $k_\perp\rho_{ih} = 1.96$ (black). The green asterisk indicates the wave frequency in the plasma rest frame measured by MMS. (b) Same as (a) for the growth rate instead of frequency. The green line indicates the measured $k_{||,Bellan}$. (c) Alfvén branch dispersion surface. The colorbar indicates normalized growth rate (γ/Ω_i). The green asterisk indicates the wave frequency in the plasma rest frame and $k_{||}$ measured by MMS. (d) Same as (c) but the colorbar indicates the ellipticity, $\epsilon = \mathrm{Re}(iB_{\perp 2}/B_{\perp 1})$. (e-g) Comparison of normalized growth rate (e), ellipticity (f) and wave normal angle (g) as a function of normalized $k_\perp\rho_{ih}$ and n_{ic}, for the $k_{||}\rho_{ih}$ that yields maximum theoretical growth rate. The plasma parameters are specified in Table S2 of the supplemental material.

term are in phase and anti-phase in the $\hat{\mathbf{e}}_{\perp 2}$ and $\hat{\mathbf{e}}_{\perp 1}$ directions, respectively, and self-consistently allow for large ellipticity and right-handed polarization of $\mathbf{\Delta E}$, without strong damping associated.

Three characteristic length-scales are considered for protons: the proton inertial length (d_i), the cold proton gyroradius (ρ_{ic}) and the hot proton gyroradius (ρ_{ih}). We compare them to the wave number and find $k_\perp d_i = 1.4$, $k_\perp \rho_{ic} = 0.12$ and $k_\perp \rho_{ih} = 1.9$. Only the cold proton gyroradius is significantly smaller than the characteristic scale of the wave, and this would explain why the hot protons are, to a large extent, demagnetized (note, however, that the demagnetization of the hot protons is not fully achieved; see Figures 2e and 2j). The ratio $k_\perp \rho_{ic} << 1$ is consistent with the observed cold proton magnetization, indicating that cold protons gyration occurs at a scale much smaller than the perpendicular wavelength. It is interesting to see that cold protons remain fully frozen-in, despite $k_\perp d_i = 1.4$. We expect that cold protons would also be demagnetized for larger $k_\perp d_i$. Since the cold protons remain frozen-in, it is not expected that they will be significantly heated, consistent with the observations by B. J. Anderson and Fuselier (1994). In summary, the wave-proton interaction is in a hybrid regime, with the cold proton population interacting as a fluid and the hot proton population interacting kinetically.

The wave was observed very close to the reconnecting magnetopause, and therefore it is likely that the source of energy was compressions of the magnetosphere driven by solar wind pressure pulses, resulting in the observed hot ion temperature anisotropy (e.g., B. Anderson & Hamilton, 1993; Engebretson et al., 2015). These waves can, in turn, accelerate and heat some of the magnetospheric ion populations, particularly heavy ions (e.g., Tanaka, 1985; Zhang et al., 2011), potentially acting as a preconditioning process of the plasma inflowing towards the reconnecting magnetopause.

We showed detailed four-spacecraft measurements inside an EMIC wave near the reconnecting magnetopause reconnection and provided observational evidence of the different dynamics of cold and hot protons. They interact in a fluid and kinetic fashion, respectively, and this has implications for the electric fields and currents that the wave sets, self-consistently favoring wave generation and propagation at oblique angles with highly-elliptical right-handed polarization, due to the cold ion term in the Ohm's law. This provides a possible explanation for the predominance of highly elliptical and right-handed polarization EMIC waves in the Earth's magnetosphere (e.g., Min et al., 2012; Allen et al., 2015), which is often populated by cold ions of ionospheric origin (e.g., André & Cully, 2012).

Acknowledgments

STR acknowledges support from the ISSI international team *Cold plasma of ionospheric origin in the Earth's magnetosphere* and of the Ministry of Economy and Competitiveness (MINECO) of Spain (grant FIS2017-90102-R). Research at IRAP was supported by CNRS, CNES and the University of Toulouse. JHL and DLT acknowledge support from NASA Grant 80NSSC18K1378. RED was supported by NASA grants 80NSSC19K070 and 80NSSC19K0254. MA was supported by SNSA grant 56/18. SKV and RCA acknowledge support from NASA Grant 80NSSC19K0270. Work performed by MMS team members is supported by NASA contract NNG04EB99C. MMS data is publicly available at https://lasp.colorado.edu/mms/sdc/public/

References

Allen, R. C., Zhang, J.-C., Kistler, L. M., Spence, H. E., Lin, R.-L., Klecker, B., ... Jordanova, V. K. (2015). A statistical study of emic waves observed by cluster: 1. wave properties. *Journal of Geophysical Research: Space Physics*, *120*(7),

5574-5592.

Alm, L., André, M., Graham, D. B., Khotyaintsev, Y. V., Vaivads, A., Chappell, C. R., ... Vines, S. K. (2019). Mms observations of multiscale hall physics in the magnetotail. *Geophysical Research Letters*, *46*(17-18), 10230-10239.

Anderson, B., & Hamilton, D. C. (1993). Electromagnetic ion cyclotron waves stimulated by modest magnetospheric compressions. *Journal of Geophysical Research: Space Physics*, *98*(A7), 11369-11382.

Anderson, B. J., Denton, R. E., Ho, G., Hamilton, D. C., Fuselier, S. A., & Strangeway, R. J. (1996). Observational test of local proton cyclotron instability in the earth's magnetosphere. *Journal of Geophysical Research: Space Physics*, *101*(A10), 21527-21543.

Anderson, B. J., Erlandson, R. E., & Zanetti, L. J. (1992). A statistical study of pc 1-2 magnetic pulsations in the equatorial magnetosphere: 2. wave properties. *Journal of Geophysical Research: Space Physics*, *97*(A3), 3089-3101.

Anderson, B. J., & Fuselier, S. A. (1994). Response of thermal ions to electromagnetic ion cyclotron waves. *Journal of Geophysical Research*, *99*(A10).

André, M., & Cully, C. M. (2012). Low-energy ions: A previously hidden solar system particle population. *Geophysical Research Letters*, *39*(3), n/a-n/a.

André, M., Li, W., Toledo-Redondo, S., Khotyaintsev, Y. V., Vaivads, A., Graham, D. B., ... Saito, Y. (2016). Magnetic reconnection and modification of the hall physics due to cold ions at the magnetopause. *Geophysical Research Letters*, *43*(13), 6705-6712.

Balikhin, M. A., Pokhotelov, O. A., Walker, S. N., Amata, E., Andre, M., Dunlop, M., & Alleyne, H. S. C. K. (2003). Minimum variance free wave identification: Application to cluster electric field data in the magnetosheath. *Geophysical Research Letters*, *30*(10).

Bellan, P. M. (2016). Revised single-spacecraft method for determining wave vector k and resolving space-time ambiguity. *Journal of Geophysical Research: Space Physics*, *121*(9), 8589-8599.

Burch, J. L., Moore, T. E., Torbert, R. B., & Giles, B. L. (2015). Magnetospheric multiscale overview and science objectives. *Space Science Reviews*, *199*(1-4), 5-21.

Cassak, P. A., & Shay, M. A. (2007). Scaling of asymmetric magnetic reconnection: General theory and collisional simulations. *Physics of Plasmas*, *14*(10).

Denton, R. E., Anderson, B. J., Ho, G., & Hamilton, D. C. (1996). Effects of wave superposition on the polarization of electromagnetic ion cyclotron waves. *Journal of Geophysical Research: Space Physics*, *101*(A11), 24869-24885.

Dunlop, M., Southwood, D., Glassmeier, K.-H., & Neubauer, F. (1988). Analysis of multipoint magnetometer data. *Advances in Space Research*, *8*(9-10), 273-277.

Engebretson, M. J., Posch, J. L., Wygant, J. R., Kletzing, C. A., Lessard, M. R., Huang, C. L., ... Shiokawa, K. (2015). Van allen probes, noaa, goes, and ground observations of an intense emic wave event extending over 12 h in magnetic local time. *Journal of Geophysical Research: Space Physics*, *120*(7), 5465-5488.

Ergun, R. E., Tucker, S., Westfall, J., Goodrich, K. A., Malaspina, D. M., Summers, D., ... Cully, C. M. (2014). The axial double probe and fields signal processing for the mms mission. *Space Science Reviews*, *199*(1-4), 167-188.

Gary, S. P. (1992). The mirror and ion cyclotron anisotropy instabilities. *Journal of Geophysical Research*, *97*(A6).

Gary, S. P., Moldwin, M. B., Thomsen, M. F., Winske, D., & McComas, D. J. (1994). Hot proton anisotropies and cool proton temperatures in the outer magnetosphere. *Journal of Geophysical Research: Space Physics*, *99*(A12), 23603-23615.

Gary, S. P., & Winske, D. (1990). Computer simulations of electromagnetic instabilities in the plasma sheet boundary layer. *Journal of Geophysical Research*,

95(A6).

Hu, Y., & Denton, R. (2009). Two-dimensional hybrid code simulation of electromagnetic ion cyclotron waves in a dipole magnetic field. *Journal of Geophysical Research: Space Physics*, *114*(A12).

Hu, Y., Denton, R., & Johnson, J. (2010). Two-dimensional hybrid code simulation of electromagnetic ion cyclotron waves of multi-ion plasmas in a dipole magnetic field. *Journal of Geophysical Research: Space Physics*, *115*(A9).

Kennel, C. F., & Petschek, H. (1966). Limit on stably trapped particle fluxes. *Journal of Geophysical Research*, *71*(1), 1-28.

Lee, J. H., Turner, D. L., Toledo-Redondo, S., Vines, S. K., Allen, R. C., Fuselier, S. A., ... Burch, J. L. (2019). Mms measurements and modeling of peculiar electromagnetic ion cyclotron waves. *Geophysical Research Letters*, *46*(21), 11622-11631.

Li, W. Y., André, M., Khotyaintsev, Y. V., Vaivads, A., Fuselier, S. A., Graham, D. B., ... Burch, J. (2017). Cold ionospheric ions in the magnetic reconnection outflow region. *Journal of Geophysical Research: Space Physics*, *122*(10), 10,194-10,202.

Lindqvist, P. A., Olsson, G., Torbert, R. B., King, B., Granoff, M., Rau, D., ... Tucker, S. (2014). The spin-plane double probe electric field instrument for mms. *Space Science Reviews*, *199*(1-4), 137-165.

Min, K., Lee, J., Keika, K., & Li, W. (2012). Global distribution of emic waves derived from themis observations. *Journal of Geophysical Research: Space Physics*, *117*(A5), n/a-n/a.

Omidi, N., Thorne, R., & Bortnik, J. (2011). Hybrid simulations of emic waves in a dipolar magnetic field. *Journal of Geophysical Research: Space Physics*, *116*(A9).

Pinçon, J.-L., & Glassmeier, K.-H. (2008). Multi-spacecraft methods of wave field characterisation. *ISSI Scientific Reports Series*, *8*, 47.

Pollock, C., Moore, T., Jacques, A., Burch, J., Gliese, U., Saito, Y., ... Zeuch, M. (2016). Fast plasma investigation for magnetospheric multiscale. *Space Science Reviews*, *199*(1-4), 331-406.

Roennmark, K. (1982). *Whamp - waves in homogeneous, anisotropic, multicomponent plasmas* (Tech. Rep.).

Russell, C. T., Anderson, B. J., Baumjohann, W., Bromund, K. R., Dearborn, D., Fischer, D., ... Richter, I. (2014). The magnetospheric multiscale magnetometers. *Space Science Reviews*, *199*(1-4), 189-256.

Shi, C., Zhao, J., Huang, C., Wang, T., & Dunlop, M. W. (2020). Modulation of ionospheric outflow ions by emic waves in the dayside outer magnetosphere. *Physics of Plasmas*, *27*(3).

Tanaka, M. (1985). Simulations of heavy ion heating by electromagnetic ion cyclotron waves driven by proton temperature anisotropies. *Journal of Geophysical Research*, *90*(A7).

Thorne, R., & Horne, R. (1993). Cyclotron absorption of ion-cyclotron waves at the bi-ion frequency. *Geophysical research letters*, *20*(4), 317-320.

Toledo-Redondo, S., André, M., Khotyaintsev, Y. V., Lavraud, B., Vaivads, A., Graham, D. B., ... Burch, J. L. (2017). Energy budget and mechanisms of cold ion heating in asymmetric magnetic reconnection. *Journal of Geophysical Research: Space Physics*, *122*(9), 9396-9413.

Toledo-Redondo, S., André, M., Khotyaintsev, Y. V., Vaivads, A., Walsh, A., Li, W., ... Russell, C. T. (2016). Cold ion demagnetization near the x-line of magnetic reconnection. *Geophysical Research Letters*, *43*(13), 6759-6767.

Toledo-Redondo, S., Vaivads, A., André, M., & Khotyaintsev, Y. V. (2015). Modification of the hall physics in magnetic reconnection due to cold ions at the earth's magnetopause. *Geophysical Research Letters*, *42*(15), 6146-6154.

Toledo-Redondo, S., Dargent, J., Aunai, N., Lavraud, B., André, M., Li, W., ...

Burch, J. L. (2018). Perpendicular current reduction caused by cold ions of ionospheric origin in magnetic reconnection at the magnetopause: Particle-in-cell simulations and spacecraft observations. *Geophysical Research Letters*, *45*(19), 10,033-10,042.

Toledo-Redondo, S., Lavraud, B., Fuselier, S. A., André, M., Khotyaintsev, Y. V., Nakamura, R., ... Burch, J. L. (2019). Electrostatic spacecraft potential structure and wake formation effects for characterization of cold ion beams in the earth's magnetosphere. *Journal of Geophysical Research: Space Physics*, *124*(12), 10048-10062.

Trattner, K., Mulcock, J., Petrinec, S., & Fuselier, S. (2007). Probing the boundary between antiparallel and component reconnection during southward interplanetary magnetic field conditions. *Journal of Geophysical Research: Space Physics*, *112*(A8).

Young, D. T., Burch, J. L., Gomez, R. G., De Los Santos, A., Miller, G. P., Wilson, P., ... Webster, J. M. (2014). Hot plasma composition analyzer for the magnetospheric multiscale mission. *Space Science Reviews*, *199*(1-4), 407-470.

Zhang, J. C., Kistler, L. M., Mouikis, C. G., Klecker, B., Sauvaud, J. A., & Dunlop, M. W. (2011). A statistical study of emic wave-associated he+energization in the outer magnetosphere: Cluster/codif observations. *Journal of Geophysical Research: Space Physics*, *116*(A11), n/a-n/a.